Dimerization and DNA-Binding Properties of the Transcription Factor ΔFosB†

Helena J. M. M. Jorissen,‡ Paula G. Ulery,§ Lisa Henry,|| Sreekrishna Gourneni,‡ Eric J. Nestler,§ and Gabby Rudenko*,‡,⊥

Life Sciences Institute, University of Michigan, 210 Washtenaw Avenue, Ann Arbor, Michigan 48109-2216, Department of Psychiatry and Biochemistry, The University of Texas (UT) Southwestern Medical Center at Dallas, 5323 Harry Hines Boulevard, Dallas, Texas 75390, Howard Hughes Medical Institute (HHMI), 4000 Jones Bridge Road, Chevy Chase, MD 20815-6789, and Department of Pharmacology, University of Michigan Medical School, 1301 MSRB III, 1150 West Medical Center Drive, Ann Arbor, Michigan 48109-0632

Received March 12, 2007; Revised Manuscript Received May 7, 2007

ABSTRACT: The transcription factor, ΔFosB, a splice isoform of fosB, accumulates in rodents in a brain-region-specific manner in response to chronic administration of drugs of abuse, stress, certain antipsychotic or antidepressant medications, electroconvulsive seizures, and certain lesions. Increasing evidence supports a functional role of such ΔFosB induction in animal models of several psychiatric and neurologic disorders. Fos family proteins, including ΔFosB, are known to heterodimerize with Jun family proteins to create active AP-1 transcription-factor complexes, which bind to DNA specifically at AP-1 consensus sites. We show here, using a range of biochemical and biophysical means, that recombinant, purified ΔFosB forms homodimers as well, at concentrations less than 500 nM, and that these homodimers specifically bind to DNA oligonucleotides containing AP-1 consensus sequences in the absence of any Jun partner. Our results suggest that, as ΔFosB accumulates to abnormally elevated protein levels in highly specific regions of the brain in response to chronic stimulation, functional homodimers of ΔFosB are formed with the potential to uniquely regulate patterns of gene expression and thereby contribute to the complex processes of neural and behavioral adaptation.

Members of the Fos and Jun families of transcription factors are induced in the rodent brain upon administration of a large variety of stimuli (*1*, *2*). Numerous studies have shown that a single acute stimulus leads to the rapid but very short-lived induction of mRNA and protein for c-Fos, FosB, and JunB in specific, stimulus-associated brain regions, while mRNA levels for JunD and c-Jun are usually not elevated. In contrast, chronic administration of these various stimuli leads to a very different pattern of Fos/Jun expression (*3*, *4*). Induction of c-Fos and JunB and to a lesser extent FosB desensitize, while ΔFosB protein, a truncated product of the fosB gene, remains uniquely elevated for weeks after the last chronic stimulus because of the unusual stability of the protein (*5*−*7*). Increasing evidence supports the functional importance of ΔFosB induction in animal models of several psychiatric and neurologic disorders (*4*).

While Jun proteins homodimerize as well as heterodimerize with Fos family proteins to form active AP-1 transcription-factor complexes, Fos proteins are thought to form only heterodimers with a Jun partner (*1*, *2*). These AP-1 complexes then bind to AP-1 sites present in the regulatory regions of many genes to regulate their transcription. Through alternative splicing of the fosB pre-mRNA, ΔFosB lacks the 101 C-terminal residues found in FosB. However, the DNA-binding and leucine zipper dimerization domains are fully intact in ΔFosB. Accordingly, ΔFosB binds radiolabeled oligonucleotides containing an AP-1 site in gel-shift assays (see the Discussion), and chromatin immunoprecipitation (ChIP) of brain extracts has confirmed ΔFosB binding to specific, regulated genes in vivo (*8*). In addition, ΔFosB induction has been shown to regulate the expression of numerous functionally important target genes in the brain in vivo [(*9*), see the Discussion].

However, despite its functional importance, little is known about the biochemical properties of ΔFosB. Also, it is striking that the accumulation of ΔFosB in the brain after chronic stimulation occurs in the absence of induction of any Jun family protein, which has raised questions about the nature of ΔFosB action in vivo. We, therefore, embarked on studies to characterize ΔFosB in an isolated, purified state. His-tagged ΔFosB, derived from insect cells, was analyzed in terms of molecular weight, oligomerization state, and DNA-binding properties. Our studies reveal that ΔFosB has the potential to act independently of Jun proteins, because it forms dimers at concentrations lower than 500 nM and is able to selectively bind DNA oligonucleotides containing AP-1 consensus sequences. Our results raise the novel possibility that the accumulation of just ΔFosB in neurons

† This work was supported by a National Alliance for Research on Schizophrenia and Depression Young Investigator Award, an American Heart Association Scientist Development Award, and funds from the Life Sciences Institute, University of Michigan awarded to G.R., as well as grants from the National Institute for Mental Health to G.R. and E.J.N.

* To whom correspondence should be addressed: Life Sciences Institute, University of Michigan Medical School, 210 Washtenaw Ave., Rm 3161A, Ann Arbor, Michigan 48109-2216. Telephone: (734) 615-9323. Fax: (734) 763-6492. E-mail: rudenko@umich.edu.

‡ University of Michigan.

§ UT Southwestern Medical Center at Dallas.

|| HHMI.

⊥ University of Michigan Medical School.

10.1021/bi700494v CCC: $37.00
Published on Web 06/20/2007

in response to chronic stimuli is sufficient to trigger downstream effects. Once ΔFosB protein levels reach a critical threshold, past which functional homodimers of ΔFosB are formed, these would regulate gene expression and contribute to the complex process of neural adaptation.

MATERIALS AND METHODS

Overexpression of N(His)$_6$ΔFosB. ΔFosB from mouse (a splice form of fosB, accession number P13346) was expressed as an N-terminally His-tagged protein in insect cells exploiting the Invitrogen Bac-to-Bac system according to the instructions of the manufacturer. The recombinant protein contains the N-terminal tag MGHHHHHHAG followed by residues (F^2−E^{237}) from ΔFosB. The secondary virus was plaque-purified and amplified to generate large quantities of high titer tertiary virus suitable for infection of large-scale insect cultures ($1.0-5.0 \times 10^8$ pfu/mL). For overexpression, 6 L of Sf9 cells grown in SF900 medium (containing 1:200 antibiotics/antimycotics) was infected at a cell density of 1.5×10^6 cells/mL, with a multiplicity of infection (MOI) of 1.5, and incubated for 72−76 h at 28 °C and 145 rpm. The 6 L cells were harvested by centrifugation for 10 min at 2000*g* and 4 °C, resuspended in 50 mL of 1× phosphate-buffered saline (PBS), and flash-frozen in liquid nitrogen.

Purification of N(His)$_6$ΔFosB. Cells from 6 L cultures were thawed and resuspended in 150 mL of lysis buffer [20 mM Tris at pH 7.5, 0.2% Triton X-100, 1 mM TCEP, 0.5 mM PMSF, 10 μg/mL leupeptin, 1 μg/mL pepstatin A, and 1 Complete ethylenediaminetetraacetic acid (EDTA)-free protease inhibitor cocktail tablet containing serine and cysteine protease inhibitors (Roche)] to an end volume of 200 mL. The cells were incubated on ice for 30 min and then homogenized 25 times using a dounce homogenizer in 35 mL aliquots. NaCl was added to the lysate to an end concentration of 300 mM, as well as $MgCl_2$ and DNase, to end concentrations of 5 mM and 30 μg/mL, respectively. The lysate was further incubated for 60 min on ice and then cleared by centrifugation for 45 min at 47800*g* and 4 °C using a Sorvall Evolution RC centrifuge and a SS-34 rotor. The salt concentration of the lysate was increased to an end concentration of 1 M NaCl and 0.5 M NaBr; the latter, a mild chaotrope, was added to disrupt DNA binding to ΔFosB. In addition, 1 mM imidazole was added to the lysate in preparation for metal-affinity chromatography to prevent nonspecific binding. The lysate was further cleared by centrifugation for 40 min at 145000*g* and 4 °C using a Sorvall Evolution RC centrifuge and a SS-34 rotor. The cleared supernatant was batch-bound to a 5 mL bed volume of Ni−NTA resin (Invitrogen, equilibrated with 20 mM Tris at pH 7.5 and 1 M NaCl) for 2 h at 4 °C. The beads were collected, then washed with 20 mM Tris at pH 7.5, 1 M NaCl, and 10 mM imidazole, and finally eluted with 20 mM Tris at pH 7.5, 1 M NaCl, and 250 mM imidazole on an AKTA FPLC (GE Healthcare). The Ni−eluate was concentrated using an Amicon Ultra [molecular weight cut-off (MWCO) of 10 kDa] and diluted 25× with 20 mM Tris at pH 7.5, 50 mM NaCl, and 5 mM dithiothreitol (DTT) to reduce the salt concentration (end buffer conditions of roughly 20 mM Tris at pH 7.5, 88 mM NaCl, 10 mM imidazole, and 5 mM DTT). Precipitated protein was removed by centrifugation for 30 min at 47800*g* and 4 °C using a Sorvall Evolution RC centrifuge and a SS-34 rotor. The protein solution was loaded on a Mono Q ion-exchange column (GE Healthcare) equilibrated with 20 mM Tris at pH 7.5, 50 mM NaCl, and 5 mM DTT and eluted using a NaCl gradient of 50 mM to 1 M NaCl. As a final step, the protein was purified on a 120 mL Superdex 200 16/60 gel-filtration column equilibrated with 20 mM Tris at pH 7.5, 1 M NaCl, and 5 mM DTT. Protein purity was assessed on 12% sodium dodecyl sulfate−polyacrylamide gel electrophoresis (SDS−PAGE) gels. Protein concentrations were determined spectroscopically at 280 nm using a molar absorption coefficient of 14 440 cm^{-1} M^{-1}, determined using the method of Pace et al. (*10*). Preparations of purified N(His)$_6$ΔFosB were tested to ensure that the ratio $A_{280\ nm}/A_{260\ nm}$ exceeded 1.5, indicating that the purified protein was devoid of DNA.

Proteolytic Mapping. Aliquots of purified N(His)$_6$ΔFosB (20 μg) were digested with α-chymotrypsin, endoproteinase Lys-C, or thrombin with a 100-fold excess of target protein to protease for 10−30 min at room temperature in 20 mM Tris at pH 7.5 and 100 mM NaCl (total volume of 50 μL). Reactions were stopped with 1 mM PMSF, 0.1 mM leupeptin, and 1 mM PMSF, respectively. Half of each digest was subject to analysis by mass spectrometry, and the other half was analyzed on 12% SDS−PAGE Biorad Ready gels (Biorad). For N-terminal sequencing, identical digests were carried out in parallel, subject to SDS−PAGE, and electroblotted to Immobilon P membranes (Millipore) using standard protocols and the relevant bands were excised.

Size-Exclusion Chromatographic Analysis. Varying amounts of N(His)$_6$ΔFosB protein (2, 7, and 9 mg) in 20 mM Tris at pH 7.5, 100 NaCl, and 5 mM DTT were concentrated, centrifuged for 10 min at 13 000 rpm, and loaded in a 2 mL sample volume on a 120 mL Superdex 200 16/60 gel-filtration column equilibrated under low-salt conditions (20 mM Tris at pH 7.5, 100 mM NaCl, and 5 mM DTT) or high-salt conditions (20 mM Tris at pH 7.5, 1 M NaCl, and 5 mM DTT) with a flow rate of 0.5 mL/min. To estimate the apparent molecular weight of the species eluting, the gel-filtration column equilibrated in 20 mM Tris at pH 7.5, 1 M NaCl, 5 and mM DTT was calibrated with a set of standard proteins (Sigma; 200, 66, 29, and 12.4 kDa) loaded in a 1 mL sample volume and separated with a flow rate of 0.5 mL/min.

Electrophoretic Mobility (Gel) Shift Assays (EMSA). Double-stranded oligonucleotides (discussed in the Results and Table 3) were formed by mixing equivalent volumes of complementary single-stranded oligonucleotides (Sigma GenoSys) (1 mM stock solutions dissolved in 10 mM Tris at pH 8.0 and 50 mM NaCl) and heating the mixture to 95 °C for 2.5 min in a water bath, followed by slow cooling to room temperature (roughly 1 min/°C).

DNA-binding experiments were performed with digoxigenin (DIG)-labeled oligonucleotides. The DIG gel-shift kit, second generation (Roche), was used to label oligonucleotides at the 3′ end with DIG-ddUTP and probe protein/DNA binding. Labeled oligonucleotides were diluted to a concentration of 0.5 pmol/μL in TEN buffer (10 mM Tris at pH 8, 1 mM EDTA, and 100 mM NaCl) and stored at −20 °C. DNA binding to N(His)$_6$ΔFosB was performed in 20 μL reaction mixtures containing 50 nM of labeled oligo (1 pmol) in TEN buffer and protein diluted in TEN buffer in the range of 0−315 nM dimers of N(His)$_6$ΔFosB (i.e., 0−6.3 pmol). The protein/DNA mixtures were incubated for

10 min at room temperature. The final binding mixtures using the reagents from the gel-shift kit contained 2.8 mM Tris, 20 mM Hepes at pH 7.6, 25 mM NaCl, 30 mM KCl, 1.6 mM EDTA, 1 mM DTT, 10 mM $(NH_4)_2SO_4$, 0.2% (w/v) Tween 20, 4 mM cacodylate, 5 μg/mL bovine serum albumin (BSA), 0.1 mM $CoCl_2$, 1 μM DIG-ddUTP, 60 μM KP_i, 1 μM 2-mercaptoethanol, 0.0005% Triton X-100, and 0.05% glycerol. After incubation, 5 μL of 5× Hi-Density loading buffer (1.25× TBE, 15% ficoll, 0.1% bromophenol blue) was added to the 20 μL binding reaction and the samples were loaded on a native 6% acrylamide gel (prerun for 30 min at 50 V) in 0.5× TBE (44.5 mM Tris, 44.5 mM boric acid, and 1 mM EDTA at pH 8.3) and run at 70 V for about 1.5 h at 4 °C. The protein/DNA complex was electroblotted from the gel onto a positively charged nylon membrane (Roche) in 0.5× TBE at 400 mA (~30 V) for 60 min at 4 °C, and the blot was baked subsequently at 120 °C for 20−30 min to fix the protein/DNA complex to the membrane. Chemiluminescence detection was performed according to the protocol of the manufacturer, incubating the membrane with an anti-digoxigenin-AP antibody conjugate (1:10 000 dilution) and finally incubating the membrane with a 0.1 mg/mL solution of disodium 3-(4-methoxyspiro{1,2-dioxetane-3,2′-(5′-chloro)trichloro[3.3.1.13,7]decan}-4-yl) phenyl phosphate (CSPD), in a hybridization bag. The membranes were exposed to X-ray film (Kodak BioMax Light) for 10 min. For quantification purposes, the membranes were scanned with a Typhoon 9410 scanner (Amersham) at high sensitivity and 900 V and then analyzed using ImageQuant 5.2 software. The chemiluminescent signal recorded from the EMSA experiments with the Typhoon scanner was found to be nonlinear as a function of DIG-labeled oligonucleotide. This is likely caused by several factors, including the nonlinear transfer efficiency of both free oligonucleotide and DNA/protein complexes, as well as the nonequilibrium conditions for the binding reactions during electrophoresis, resulting, for example, in the presence of species migrating at positions other than the complex or free oligonucleotide. Therefore, EMSA gels, while qualitatively informative, could not be accurately quantified.

For competition assays, $N(His)_6\Delta FosB$:DIG-labeled DNA complexes were generated as described above containing 50 nM of DIG-labeled oligo (1 pmol) and a 210 nM dimer concentration of $N(His)_6\Delta FosB$ (4.2 pmol) in TEN buffer, i.e., conditions saturating the protein with DNA. Three different protein/DNA complexes were formed with the DIG-labeled oligonucleotides: cyclin-dependent kinase 5 (CDK5), the AMPA glutamate receptor subunit GluR2, and metallothionein (MET). To assess the specificity of DNA binding to $N(His)_6\Delta FosB$, 1 μL of unlabeled specific oligonucleotide (CDK5, GluR2, or MET) or 1 μL of unlabeled nonspecific (scrambled) oligonucleotide (SCR) was added to the protein/DNA complex reaction (containing 10, 50, 200, or 500 pmol, i.e., a 10, 50, 200, or 500 molar excess) and incubated for 15 min at room temperature. The final competition reaction contained identical buffer components as described above for the binding reactions. The samples were subject to electrophoresis, electroblotting, and chemiluminescent visualization as described above. Competition upon the addition of unlabeled oligonucleotide was monitored through the decrease of the visible protein complex and the concomitant increase in free DIG-labeled oligo in EMSA assays.

The specific activity of $N(His)_6\Delta FosB$ was determined by incubating 2.1 pmol of $N(His)_6\Delta FosB$ (dimers) with an excess of labeled GluR2 oligonucleotide (12 pmol) in a 10 μL reaction volume. While the protein was not completely saturated under these conditions, higher amounts of labeled oligonucleotide could not be used because of oligonucleotide concatemer formation. After EMSA, as described above, the background corrected signal of the protein/DNA complex was compared to the signal from a calibration series of 0−3 pmol of free labeled oligonucleotide and quantified. The results indicate that the $N(His)_6\Delta FosB$ purified from insect cells is at least 80% active (assuming that the protein binds as a dimer).

Fluorescence Anisotropy. Fluorescence anisotropy was performed with TAMRA-labeled oligonucleotides CDK5, GluR2, and SCR. 5′-TAMRA-labeled sense and anti-sense oligomers (Invitrogen) were annealed in 10 mM Tris at pH 8.0 and 50 mM NaCl at a final concentration of 50 μM by heating the mixture to 95 °C for 2.5 min in a waterbath, followed by slow cooling to room temperature (roughly 1 min/°C). Stock solutions of 100 nM double-labeled double-stranded TAMRA oligonucleotides were made in 20 mM Hepes at pH 7.5, 50 mM NaCl, and 1 mM DTT. Stock solutions of a 0−500 nM dimer concentration of $N(His)_6\Delta FosB$ were made in the same buffer. A total of 100 μL of each DNA stock solution and 100 μL of each protein stock solution were mixed in a 96-well nonbinding-surface microtiter plate (Corning) to generate a concentration series of a 0−250 nM dimeric concentration of $N(His)_6\Delta FosB$ and a fixed concentration of 50 nM labeled DNA. After incubation at room temperature for 15 min, 30 μL of each sample (in 6-fold) was transferred to a 384-well round-bottom low-volume black microtiter plate (Corning). Fluorescence anisotropy was measured using a Pherastar plate reader (BMG Labs), with excitation at 540 nm, emission at 590 nm, 100 flashes per well, and the target set to 30 mP for each individual TMR-oligo by adjusting the gain on a well with oligonucleotide in the absence of protein. Data were processed using Prism 3.0 (GraphPad Software). Each data point represents the mean of six replicates, and the error bar represents the standard deviation of the mean. The fluorescence anisotropy observed for the free oligonucleotide concentration (i.e., no protein) was set as the baseline value and subtracted from the values measured for the oligonucleotide in the presence of varying amounts of protein. The binding curves were fit with a sigmoidal curve in Prism.

Analytical Ultracentrifugation (AUC). The oligomerization state of $N(His)_6\Delta FosB$ was analyzed using AUC in sedimentation velocity and sedimentation equilibrium experiments. Additionally, as test cases with a known answer, the proteins, bovine serum albumin (Sigma) and lysozyme (Sigma), were analyzed in parallel. To prepare for the AUC experiments, $N(His)_6\Delta FosB$ and BSA were subjected to gel filtration (Superdex 200 16/60 in 20 mM Tris at pH 7.5 and 500 mM NaCl, with 5 mM DTT for $N(His)_6\Delta FosB$ and without DTT for BSA).

$N(His)_6\Delta FosB$, BSA, and lysozyme were dialyzed against at least a 100-fold volume buffer for at least 12 h at 4 °C in a standard high-salt buffer (20 mM Tris at pH 7.5, 500 mM NaCl, and 0.2 mM DTT), a low-salt buffer (20 mM Tris at pH 7.5, 100 mM NaCl, and 0.2 mM DTT), or a denaturing buffer (20 mM Tris at pH 7.5, 500 mM NaCl, 0.2 mM DTT,

and 6 M guanidine hydrochloride). Aliquots of dialysis buffer were used in the AUC reference cells to measure the protein samples with respect to their identical buffers. Dialyzed protein stock solutions with $A_{280\ nm}$ close to 1.0 were sequentially diluted with dialysis buffer to an absorbance of $A_{280\ nm} = 0.8$, 0.5, and 0.25 and, for the low concentrations, further diluted to the theoretical absorbances of $A_{280\ nm} = 0.03$, 0.015, and 0.009. For sedimentation velocity, the following N(His)$_6$ΔFosB concentrations (assuming monomers) were analyzed: 18.7, 37.4, and 69.3 μM. For sedimentation equilibrium, the following concentrations were analyzed assuming monomers of N(His)$_6$ΔFosB, 0.6, 1, 2, 17.3, 34.6, and 55.4 μM; BSA, 0.21, 0.35, 0.70, 5.9, 11.6, and 18.6 μM; and lysozyme, 0.24, 0.40, 0.79, 6.6, 13.2, and 21.1 μM.

All experiments were carried out in a Beckman Optima XL-I analytical ultracentrifuge equipped with an An50 Ti rotor, using either 2-channel (for sedimentation velocity) or 6-channel (for sedimentation equilibrium) sample cells with 12 mm path-length, charcoal-filled Epon centerpieces and either sapphire (for measurements at 280 nm) or quartz (for measurements at 230 nm) windows. Sample cells and the rotor were precooled overnight or at least for 60 min at 4 °C; the sample cells were loaded with protein and reference buffers and then precooled again in the centrifuge at 3000 rpm at 4 °C. After the temperature reached the set value of 4 °C (about 2 h), the samples were left at 3000 rpm and 4 °C for an additional 60 min before starting the experiment. Sedimentation velocity experiments were run at 40 000 or 50 000 rpm at 4 °C for 800 min (13.3 h). Data were collected every 5 min using a scan step size of 0.003 cm. Sedimentation equilibrium experiments were run at speeds of 8000 rpm (60 h), 15 000 rpm (56 h), and 25 000 rpm (30 h) at 4 °C. Equilibrium was considered established when successive scans with at least 6 h intervals resulted in overlapping plots. The data collected represent an average of 50 scans at a scan step size of 0.001 cm.

Partial specific volumes for the proteins and buffer densities were calculated with SEDNTERP 1.04 (*11*). The partial specific volume for N(His)$_6$ΔFosB is 0.7080 mL/g at 4 °C and 0.7148 mL/g at 20 °C; for BSA, 0.7258 mL/g at 4 °C and 0.7326 mL/g at 20 °C; and for lysozyme, 0.7097 mL/g at 4 °C and 0.7165 mL/g at 20 °C. The high-salt buffer (20 mM Tris at pH 7.5, 500 mM NaCl, and 0.2 mM DTT) has an estimated density of 1.019 24 g/mL at 20 °C and 1.021 04 g/mL at 4 °C; the low-salt buffer (20 mM Tris at pH 7.5, 100 mM NaCl, and 0.2 mM DTT) has an estimated density of 1.002 93 g/mL at 20 °C and 1.004 71 g/mL at 4 °C; and the denaturing buffer (20 mM Tris at pH 7.5, 500 mM NaCl, 0.2 mM DTT, and 6 M guanidine hydrochloride) has a density of 1.163 27 g/mL at 20 °C and 1.165 33 g/mL at 4 °C. Molar extinction coefficients at 280 nm (ϵ_{280}) were calculated for N(His)$_6$ΔFosB ($\epsilon_{280} = 14\,440$ au cm^{-1} M^{-1}), BSA ($\epsilon_{280} = 42\,930$ au cm^{-1} M^{-1}), and lysozyme ($\epsilon_{280} = 37\,970$ au cm^{-1} M^{-1}) using Pace et al. (*10*), as incorporated in SEDNTERP. Molar extinction coefficients at 230 nm (ϵ_{230}) were estimated for N(His)$_6$ΔFosB ($\epsilon_{230} = 48\,134$ au cm^{-1} M^{-1}), BSA ($\epsilon_{230} = 133\,140$ au cm^{-1} M^{-1}), and lysozyme ($\epsilon_{230} = 59\,707$ au cm^{-1} M^{-1}) using Stafford et al. (*12*), summing 6400 cm^{-1} M^{-1} for each Trp, 3689 cm^{-1} M^{-1} for each Tyr, and 80 cm^{-1} M^{-1} for each peptide bond present in the sequence.

Sedimentation velocity experiments were analyzed using SEDFIT version 9.3b (*13*), using the continuous *c*(*s*) analysis for noninteracting discrete species to calculate a distribution for the sedimenting species and their sedimentation coefficients. Baseline noise was refined using nonlinear least-squares (NLS) but not time-independent (TI) or radius-independent (RI) noise.

Separate experiments were carried out for measuring the sedimentation equilibration gradients for high protein concentrations by monitoring $A_{280\ nm}$ and for low protein concentrations by monitoring $A_{230\ nm}$. A global analysis was performed for data collected at each wavelength separately, to prevent high protein concentrations (potentially favoring oligomerization) from biasing the refinement results of the more dilute protein solutions. Sedimentation equilibrium experiments were analyzed using SEDFIT 9.3b and SEDPHAT 4.1b (*14*, *15*) in two different ways. To answer which species were present, "species analysis" was carried out by refining the molecular weight of two species with starting values 10 and 100 kDa, followed by nonlinear least-squares refinement (NLSR) of the baseline noise level of 0.005 and subsequent additional refinement of RI and TI noise, with TI noise rotor stretch. An additional analysis was carried out using the "self-association" analysis, supplying the protein concentrations in each sample cell to exploit mass conservation constraints (*15*). Monomer and dimer models were tested by setting $\log(K_a) = 0$ and fixing the molecular weight to the appropriate value. The data were refined against each model (monomer or dimer) with a cycle of NLS refinement adjusting the baseline noise and the bottom position of the cell to apply soft mass conservation restraints with a rotor stretch (*15*). Subsequent cycles of NLS refinement adjusted TI and RI noise levels, and then finally, the protein-loading concentrations were allowed to refine. Refining the protein concentration typically improved the fit between the model and experimental data significantly; however, it also masked to some extent the poorness of the fits to incorrect models by refining the protein concentrations to unrealistic values. While the concentrations of proteins used for the equilibrium runs at $A_{280\ nm}$ did not refine significantly from the input values in the case of the correct models, at $A_{230\ nm}$, small though significant differences were observed likely because of the inaccuracy of the molar extinction coefficients estimated at $A_{230\ nm}$; unrealistically large differences were seen in the case of incorrect models. Nevertheless, measurements taken at $A_{230\ nm}$ processed using the self-association procedure described above were very sensitive to the enforcement of an incorrect molecular weight. The fit of the data to the different models was evaluated graphically (Figure 4) and by monitoring the global error χ_r^2 for all data points (Tables 1 and 2).

RESULTS

Overexpression and Purification of ΔFosB. N(His)$_6$ΔFosB was overexpressed in Sf9 cells (Figure 1a). The purified protein migrates with an apparent molecular weight (M_w) of roughly 37 kDa using SDS−PAGE, more than 10 kDa larger than the predicted 26 443 Da based on the protein sequence (Figure 1b). To investigate if the larger than expected M_w was the result of aberrant migration during electrophoresis or the result of post-translational modification, N(His)$_6$ΔFosB was analyzed using mass spectrometry. Because N(His)$_6$ΔFosB

Table 1: Sedimentation Equilibrium Analysis of N(His)$_6$ΔFosB in the Range 17.3−55.4 μM

	model	Starting value [Da]	Refined Mw [Da]	χ_r^2 (n datapoints)[a]
ΔFosB M_w(calc)=26443.2 oligomerization state unknown	Species analysis – 2 species	10000 100000	**46796** 98640	0.7 (1038)
	Self-association with mass conservation	26443.2 (fixed)		72.2 (1039)
	Self-association with mass conservation	52886.4 (fixed)		3.3 (1039)
BSA M_w(calc)=66428.1 known monomer	Species analysis – 2 species	10000 100000	**55589** 174689	1.2 (809)
	Self-association with mass conservation	66428.1 (fixed)		18.6 (808)
	Self-association with mass conservation	132856.2 (fixed)		100.1 (808)
Lysozyme M_w(calc)=14306.2 known monomer	Species analysis – 2 species	10000 100000	**12943** 120537	0.4 (1129)
	Self-association with mass conservation	14306.2 (fixed)		0.5 (1128)
	Self-association with mass conservation	28612.4 (fixed)		11.0 (1074)

[a] χ_r^2 = reduced χ^2 value as a measure for the goodness of fit calculated by SEDPHAT as $\chi_r^2 = (1/N_{tot})\sum_e\sum_{i=1}^{N_e}((a_i^{(e)} - f_i^{(e)})^2/\sigma_e^2)$. $N_{tot} = \sum_e n_e$, where the index "*e*" refers to the individual experiments loaded that have n_e data points *a* modeled with the fit values *f*. The data points n_e in each experiment have an experimental error σ_e. The experimental noise per experiment was set to 0.005 signal units. $\chi_r^2 = 1$ if the experimental error χ_r^2 equals the experimental noise.

was not detected using electrospray ionization mass spectrometry likely because of poor ionization efficiency, matrix-assisted laser desorption ionization time-of-flight (MALDI−TOF) mass spectrometry was used to determine the molecular weight of the full-length protein even though this method is typically less accurate (±1% of the M_w). N(His)$_6$ΔFosB was found to have a M_w of 26 505 Da, with an almost equally intense signal for a species at 55 268 Da. Analyses in the presence of 5 mM TCEP, 5 mM DTT, or 20 mM DTT, to prevent potential intermolecular disulfide bond formation, yielded similar results (respectively, 26 241 Da, 26 277 Da with a very minor species at 52 960 Da, or 26 220 Da with a very minor species at approximately 52 900 Da). It appears, therefore, that N(His)$_6$ΔFosB is not post-translationally modified in insect cells by large moieties accounting for the 10 kDa shift in electrophoretic mobility or that such moieties dissociate from the protein during mass spectrometry analysis.

To confirm the mass spectroscopic analysis on N(His)$_6$ΔFosB, we generated fragments of N(His)$_6$ΔFosB through limited proteolysis. The enzymes, endoproteinase Lys-C, α-chymotrypsin, and thrombin, generated fragments that, when combined, completely spanned the full-length N(His)$_6$ΔFosB. The fragments were unambiguously assigned through a combination of electrospray ionization mass spectrometry and N-terminal sequencing of SDS−PAGE-purified, electroblotted fragments (Figure 1c). Proteolytic mapping confirmed that N(His)$_6$ΔFosB as produced by Sf9 cells is not post-translationally modified and that the residues 122−237, which contain the bZIP (basic region leucine zipper) domain of the protein, migrate at a larger than expected molecular weight on SDS−PAGE gels presumably because of the high content of charged residues (*16, 17*).

ΔFosB Forms Homodimers in Solution. To investigate the oligomerization state of N(His)$_6$ΔFosB, size-exclusion chromatography was performed (Figure 2). While small amounts of N(His)$_6$ΔFosB (<2 mg) migrate as a single species under low-salt conditions with an apparent molecular weight of 190 kDa (Figure 2a), larger quantities of the protein form aggregates under low-salt conditions with an apparent molecular weight of 470 kDa (Figure 2b). Increasing the salt concentration (>500 mM NaCl) when working with large quantities of N(His)$_6$ΔFosB resulted in a single well-behaved species again, with an apparent M_w of 180 kDa (shown for buffer containing 1 M NaCl; Figure 2c). Because migration of proteins during size-exclusion chromatography depends upon not only the molecular weight but also their shape and surface properties, molecular weight estimates for proteins that are highly elongated or that interact with the matrix of the gel-filtration column are notoriously unreliable.

AUC analyses were performed as an alternative to size-exclusion chromatography to determine the oligomeric state of N(His)$_6$ΔFosB free in solution. The first stage entailed using sedimentation velocity analyses to ascertain that the ΔFosB samples were homogeneous, a prerequisite for the second stage, in which we determined the molecular weight of the sedimenting species through sedimentation equilibrium analyses. Because the protein concentration gradient established in the sample cell during sedimentation equilibrium is the result of the exact balance between diffusion and

Table 2: Sedimentation Equilibrium Analysis of N(His)$_6$ΔFosB in the Range of 0.6−2 μM

	model	Starting value [Da]	Refined Mw [Da]	χ_r^2 (n datapoints)[a]
ΔFosB (Sample 1) M_w(calc)=26443.2 oligomerization state unknown	Species analysis – 2 species	10000 100000	8092 **59601**	0.09 (1022)
	Self-association with mass conservation	26443.2 (fixed)		7.0 (1024)
	Self-association with mass conservation	52886.4 (fixed)		0.4 (1024)
ΔFosB (Sample 2) M_w(calc)=26443.2 oligomerization state unknown	Species analysis – 2 species	10000 100000	**53503** 147498	0.07 (1086)
	Self-association with mass conservation	26443.2 (fixed)		14.3 (1082)
	Self-association with mass conservation	52886.4 (fixed)		0.7 (1082)
BSA M_w(calc)=66428.1 known monomer	Species analysis – 2 species	10000 100000	4058 **64826**	0.2 (1085)
	Self-association with mass conservation	66428.1 (fixed)		0.2 (1085)
	Self-association with mass conservation	132856.2 (fixed)		24.8 (1085)

[a] χ_r^2 = reduced χ^2 value as a measure for the goodness of fit calculated by SEDPHAT as $\chi_r^2 = (1/N_{tot})\sum_e\sum_{i=1}^{N_e}((a_i^{(e)} - f_i^{(e)})^2/\sigma_e^2)$. $N_{tot} = \sum_e n_e$, where the index "*e*" refers to the individual experiments loaded that have n_e data points *a* modeled with the fit values *f*. The data points n_e in each experiment have an experimental error σ_e. The experimental noise per experiment was set to 0.005 signal units. $\chi_r^2 = 1$ if the experimental error χ_r^2 equals the experimental noise.

sedimentation of protein molecules, molecular masses determined with this technique are measured entirely independent of the shape or surface properties of the protein under consideration.

To determine the homogeneity of purified N(His)$_6$ΔFosB, protein samples in the range of an 18.7−69.3 μM monomer concentration (i.e., 9.4−34.7 μM as a dimer) were subject to sedimentation velocity analysis (Figure 3a) and the data were processed with SEDFIT. The majority of the protein was observed as a single species (88%) with a sedimentation coefficient (s_{exp} value) of 1.5 (or corrected to standard conditions of $S_{water,20\ °C} = 2.4$) over the examined concentration range, while a very minor species was found with a larger sedimentation coefficient (parts b and c of Figure 3). Under low-salt buffer conditions (20 mM Tris at pH 7.5, 100 mM NaCl, and 0.2 mM DTT) at high protein concentration, N(His)$_6$ΔFosB samples aggregated during sedimentation velocity analysis, recapitulating the results obtained by size-exclusion chromatography. However, in the presence of the denaturant, 6 M guanidine hydrochloride, N(His)$_6$ΔFosB samples produced a single species more resistant to sedimentation compared to native conditions ($s_{exp} < 1$), indicating that, under native conditions, N(His)$_6$ΔFosB is more compact; i.e., elements are folded (results not shown). Finally and most importantly, the sedimentation velocity analyses indicated that, under the experimental conditions used, N(His)$_6$ΔFosB contained one predominant species suitable for additional analysis by sedimentation equilibrium.

Sedimentation equilibrium analysis was performed on N(His)$_6$ΔFosB samples in the range of a 0.6−55.4 μM monomer concentration (or 0.3−27.7 μM as dimers). Protein concentration gradients were established at three different speeds for six different N(His)$_6$ΔFosB protein concentrations (Tables 1 and 2 and Figure 4). In parallel, six different BSA protein concentrations as well as three different lysozyme concentrations were taken along as test cases (Tables 1 and 2). The equilibrium data were processed with SEDFIT/SEDPHAT using two different procedures as described in detail in the Materials and Methods and briefly below.

First, rough estimates of the molecular weight of ΔFosB were calculated, permitting the presence of two species to accommodate a scenario of a major species and a minor species (because of the presence of aggregated protein, proteolytic fragments, nonrelated contaminating proteins, or noise that would otherwise distort the molecular-weight calculations). At both high protein concentrations (17−55 μM of the monomer; Table 1) and low protein concentrations (0.6−2 μM of the monomer; Table 2), only one consistent molecular weight was found for N(His)$_6$ΔFosB in the range of 47−60 kDa (see values reported for "species analysis = 2 species" in Tables 1 and 2). Results for BSA and lysozyme were consistent with their known monomeric molecular weights.

The sedimentation equilibrium data were processed in a second manner by testing if the data were better fit by a monomeric or dimeric model [i.e., M_w of 26 443 or 52 886

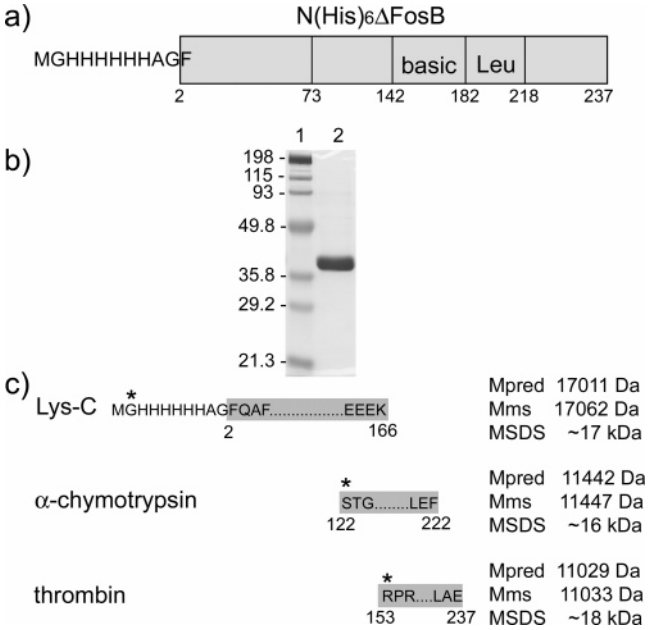

FIGURE 1: N(His)$_6$ΔFosB. (a) Schematic of N(His)$_6$ΔFosB. Two regions comprising the "bZIP" domain are indicated, one rich in basic residues ("basic") and the other rich in leucine residues ("Leu"). The N-terminal hexahistidine tag is indicated. (b) Overexpressed N(His)$_6$ΔFosB purified from insect cells and submitted to SDS−PAGE on a 12% SDS−PAGE Biorad Ready gel. Lane 1, Biorad prestained molecular-weight markers in a broad range (in kDa); lane 2, purified N(His)$_6$ΔFosB. (c) Proteolytic mapping of N(His)$_6$ΔFosB using endoproteinase Lys-C, α-chymotrypsin, and thrombin. For each fragment, the predicted molecular weight (M_{pred}) and the molecular weights determined by mass spectrometry (M_{ms}) and SDS−PAGE electrophoresis (M_{SDS}) are listed. An asterisk indicates the first of five residues identified for each fragment through N-terminal sequencing.

Da for N(His)$_6$ΔFosB]. The results were visualized by plotting the equilibrium data together with the different models and plotting the residual errors describing the fit between the two. Five different N(His)$_6$ΔFosB concentrations are shown in Figure 4, with a good fit (top panel) and poor fit (bottom panel). It is clear that the equilibrium data for N(His)$_6$ΔFosB were very well-described by a dimeric species but poorly described by a monomeric species. The goodness of fit (χ_r^2) between the experimental data and that predicted from a monomer or dimer model, respectively, are given in Tables 1 and 2 (values reported for "self-association with mass conservation"). Correct models (i.e., monomeric BSA and lysozyme) display good fits, while incorrect models (i.e., dimeric BSA or dimeric lysozyme) display poor fits, with χ_r^2 values up to 5−125 times higher. Equilibrium data for N(His)$_6$ΔFosB at high protein concentrations were clearly a much better fit with a dimeric model (χ_r^2 in the range of 3) compared to fitting with a monomeric model (χ_r^2 in the range of 72) (Table 1); this was also true at low protein concentrations (for two independent samples, χ_r^2 values of 0.4 and 0.7 for a dimer model versus χ_r^2 values of 7.0 and 14.0 as a monomer) (Table 2). At the lowest protein concentration (0.3 μM dimers) tested for N(His)$_6$ΔFosB, the data were also clearly better fit by a dimeric model than a monomeric model, although the data exhibited poor signal-to-noise because of the low absorbance at 230 nm. The sedimentation equilibrium studies hence convincingly indicate that N(His)$_6$ΔFosB homodimerizes in solution at concentrations extending lower than 0.5 μM dimers.

ΔFosB Can Bind DNA on Its Own. Intrigued by the dimeric form of N(His)$_6$ΔFosB in solution, we then investigated if N(His)$_6$ΔFosB is able to bind DNA fragments containing an AP-1 site. DIG-labeled oligonucleotides (19-mers) were generated on the basis of gene promotors of CDK5, MET, and GluR2 (see Table 3), three known targets of ΔFosB (*18*−*20*). In addition, a completely scrambled sequence was synthesized representing a nonspecific oligonucleotide (SCR). The CDK5, GluR2, and MET oligonucleotides have previously been shown to bind AP-1 complexes (known to comprise ΔFosB) in striatal cell lysates derived from chronic cocaine- and chronic ECS-treated rodents.

EMSA (gel-shift) assays demonstrate that N(His)$_6$ΔFosB can bind DNA in the absence of any Jun protein (Figure 5). While EMSA assays are not well-suited to determine accurate K_D values for DNA binding (because of technical limitations, including the nonequilibrium conditions of the binding, dissociation of the complex during electrophoresis, and uneven transfer during electroblotting), rough estimates were made nevertheless by monitoring the decrease in free oligonucleotide as increasing amounts of protein were titrated into the protein/DNA-binding reaction. Half-maximal binding of free oligonucleotide was estimated at dimeric concentrations of N(His)$_6$ΔFosB around 90 nM for MET and CDK5, 105 nM for GluR2, and 235 nM for SCR. More than 80% of the purified N(His)$_6$ΔFosB was estimated to be capable of binding DNA in specific activity measurements (see the Materials and Methods).

To demonstrate the specificity of DNA binding, competition assays were carried out reversing the binding of labeled oligonucleotides to N(His)$_6$ΔFosB by the addition of excess unlabeled oligonucleotide. Increasing amounts of unlabeled CDK5, MET, and GluR2 as well as the scrambled oligonucleotide SCR were assayed for their ability to disrupt an existing N(His)$_6$ΔFosB/DNA complex (lane 2 in parts a−c of Figure 6) formed with the DIG-labeled oligos CDK5, MET, or GluR2, respectively (input free oligonucleotide shown in lane 1 in parts a−c of Figure 6). The addition of 10-fold unlabeled specific oligonucleotide (CDK5) was sufficient to significantly disrupt the N(His)$_6$ΔFosB/CDK5 complex (lane 3 in Figure 6a), while the addition of 200-fold SCR oligo was required to significantly disrupt the protein/DNA complex (lane 9 in Figure 6a). Similar results were obtained using unlabeled GluR2 and MET oligonucleotides as competitors, indicating that these oligonucleotides, while less effective than the CDK5 oligonucleotide, do bind N(His)$_6$ΔFosB specifically. Likewise, significant disruption of N(His)$_6$ΔFosB/GluR2 or N(His)$_6$ΔFosB/MET was achieved with the addition of 10-fold unlabeled GluR2 or MET, respectively (lane 3 in parts b and c of Figure 6), compared to the more than 50-fold molar excess SCR oligonucleotide needed to achieve similar disruption of the respective complexes (lane 8 in parts b and c of Figure 6) (compare the amount of complex versus free oligo in each lane).

To verify the DNA-binding properties of N(His)$_6$ΔFosB in solution, we performed fluorescence anisotropy experiments using TAMRA (TMR)-labeled oligonucleotides. The increase in detectable polarized fluorescent emission was monitored as a measure of protein/DNA binding based on the phenomenon that oligonucleotides bound to protein molecules tumble slower in solution than unbound oligonucleotides, putting the former in a position to emit a more

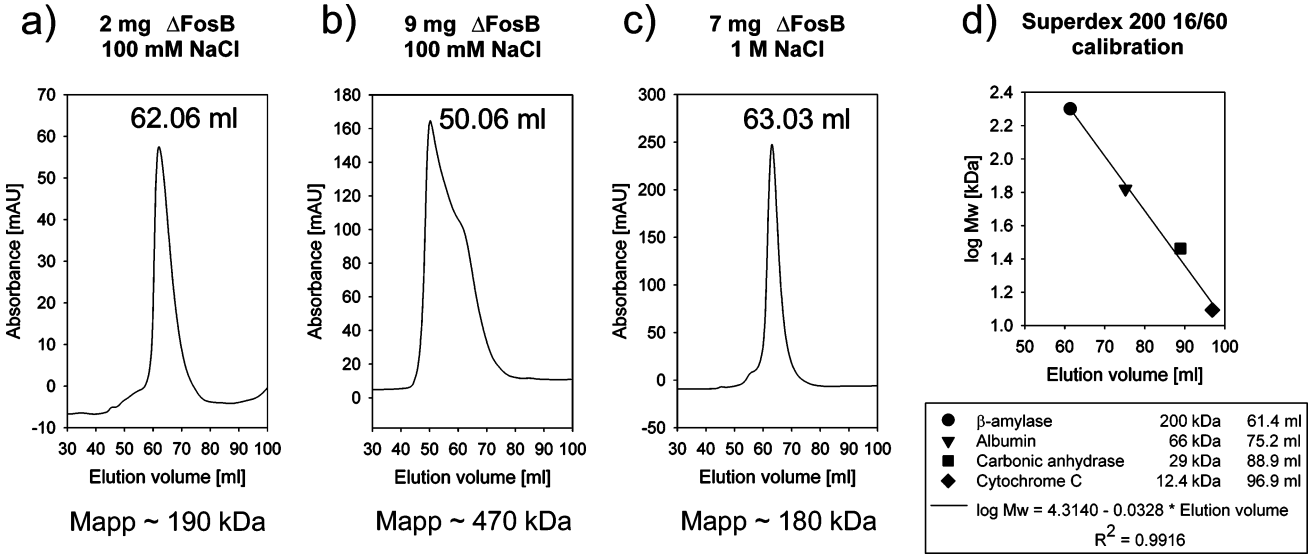

FIGURE 2: Analysis of N(His)$_6$ΔFosB with size-exclusion chromatography. The hydrodynamic radius of purified N(His)$_6$ΔFosB was analyzed on a Superdex 200 16/60 column under low-salt conditions (20 mM Tris at pH 7.5, 100 mM NaCl, and 5 mM DTT) and high-salt conditions (20 mM Tris at pH 7.5, 1000 mM NaCl, and 5 mM DTT). (a) Protein (2 mg) under low-salt conditions, (b) protein (9 mg) under low-salt conditions, (c) protein (7 mg) under high-salt conditions, and (d) elution volumes of a set of standard globular proteins (Sigma) under high-salt conditions on the same column. Molecular weights for N(His)$_6$ΔFosB were estimated (M_{app}) from these elution volumes (a−c) but serve only as a very rough guide to evaluate "large" versus "small" species (see the explanation in the Results).

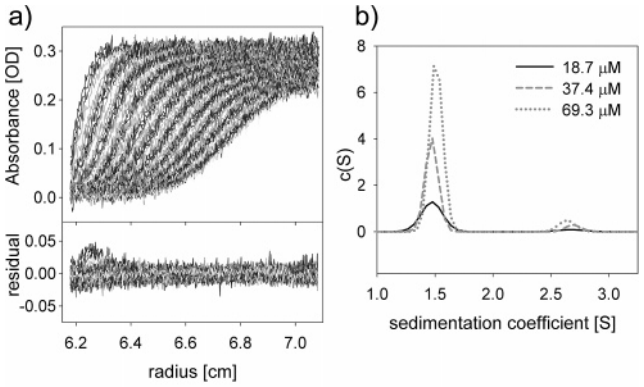

c)

	Protein [μM]	s_{exp} [10^{-13} s]	$S_{20,w}$ [10^{-13} s]
ΔFosB	18.7	1.47	2.38
	37.4	1.47	2.38
	69.3	1.51	2.44

in 20 mM Tris pH 7.5, 500 mM NaCl, 0.2 mM DTT

FIGURE 3: Sedimentation velocity analysis of N(His)$_6$ΔFosB. (a) Sedimentation velocity scans generated with an 18.7 μM monomeric concentration of N(His)$_6$ΔFosB at 50 000 rpm (top panel) and the residuals between these data and their calculated best-fit radial distributions (bottom panel), (b) distribution of species $c(s)$ as a function of the sedimentation coefficient "s_{exp}" determined at three different monomer concentrations of N(His)$_6$ΔFosB: 18.7, 37.4, and 69.3 μM, and (c) tabulation of samples analyzed by sedimentation velocity, experimental s values determined, and s values converted to standard conditions (20 °C and water).

detectable polarized signal upon excitation with polarized light than freely rotating oligonucleotides. The CDK5 and GluR2 oligonucleotides were tested as well as the scrambled oligonucleotide (SCR). N(His)$_6$ΔFosB binds TMR-CDK5 and TMR-GluR2 in a saturating manner with half-maximal binding of roughly 120 and 130 nM of dimeric N(His)$_6$ΔFosB, respectively (Figure 7a). N(His)$_6$ΔFosB does not bind TMR-SCR nearly as well. Competition with unlabeled oligonucleotides demonstrated that the N(His)$_6$ΔFosB/TMR-CDK5 complex is disrupted about 50% by a 10-fold molar excess of unlabeled CDK5, while the addition of a 10-fold molar excess of unlabeled SCR oligonucleotide only slightly disrupted the complex (Figure 7b). The addition of a 10-fold molar excess of unlabeled GluR2 oligonucleotide somewhat disrupted the N(His)$_6$ΔFosB/TMR-GluR2 complex but only slightly more so than the SCR oligo (Figure 7c). Interestingly, the DNA-binding curves in Figure 7 are sigmaoidal in shape, which may indicate cooperativity of binding (i.e., an increase in apparent DNA-binding affinity with an increasing protein concentration, as a result of concomitant dimer formation for example).

DISCUSSION

ΔFosB is an attractive candidate to mediate stable neural adaptation. ΔFosB accumulates only upon exposure to repeated and not acute stimuli and persists in the brain for relatively long periods after the last stimulation. Diverse types of chronic treatment trigger ΔFosB accumulation in a region-specific manner in the brain, including drugs of abuse (*21*−*28*), electrically and chemically induced seizures (*18*, *23*, *29*−*33*), antidepressant and antipsychotic drugs (*21*, *34*−*36*), lesions (*37*−*39*), and stress (*40*).

Increasing evidence supports the functional importance of ΔFosB induction in animal models of several psychiatric and neurologic disorders (*4*). Induction of ΔFosB by drugs of abuse in reward-related brain regions increases the sensitivity of an animal to the rewarding effects of the drugs (*20*, *41*−*43*). ΔFosB induction in dorsal striatum is related to the abnormal involuntary movements (dyskinesias) seen in models of Parkinson's disease and in response to first-generation antipsychotic drugs (*33*, *35*, *44*−*48*). In cortical regions, ΔFosB regulates the seizure threshold (*31*), and in stress-related brain regions, ΔFosB represents a positive, homeostatic mechanism that enhances the ability of an animal to cope with subsequent stresses (*49*).

What thus far has been missing is a detailed understanding of the biochemical and biophysical properties of ΔFosB.

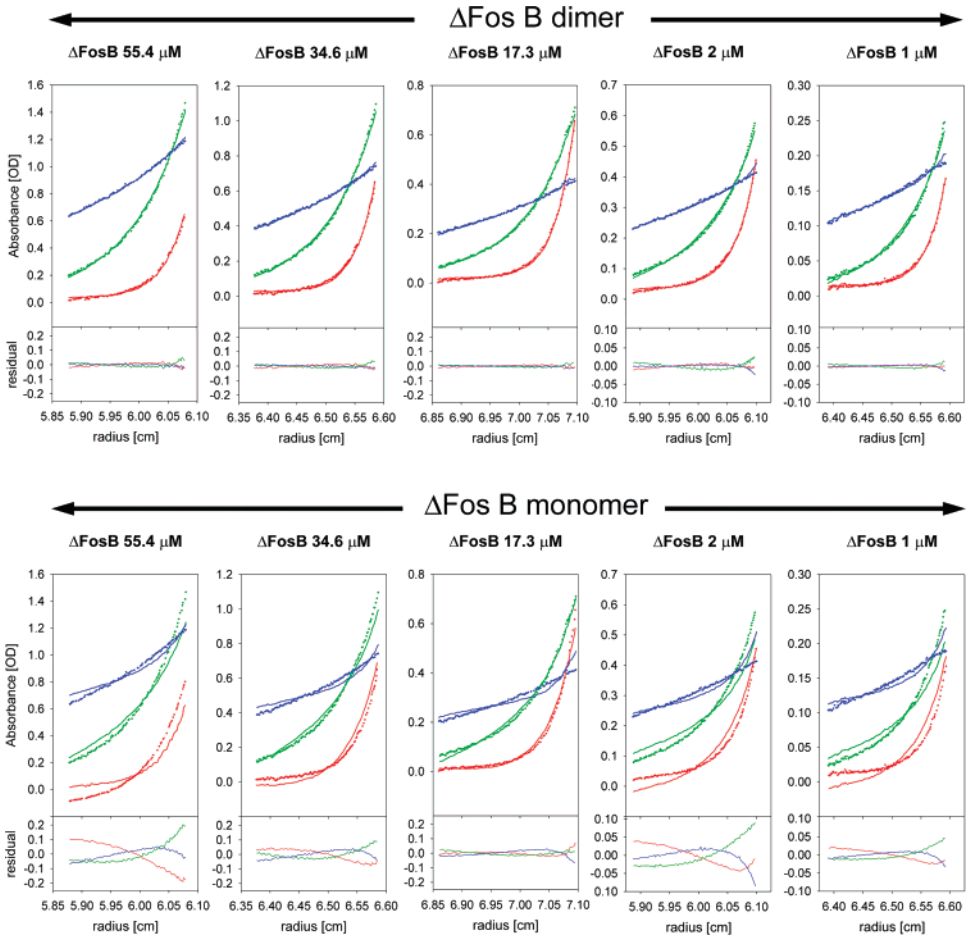

FIGURE 4: Sedimentation equilibrium analysis of N(His)$_6$ΔFosB. Sedimentation equilibrium at 8000 rpm (shown in blue), 15 000 rpm (shown in green) and 25 000 rpm (shown in red) for N(His)$_6$ΔFosB samples at monomeric concentrations of 17.3, 34.6, and 55.4 μM (measured at 280 nm) and 0.6, 1, and 2 μM (measured at 230 nm). The 0.6 μM sample is not shown because of the low signal-to-noise. The experimental data points are shown as dots, and the calculated fits are shown as lines. Data were processed assuming that N(His)$_6$ΔFosB is a dimer with M_w 52 886 Da (top panel). Data were also processed assuming that N(His)$_6$ΔFosB is a monomer with M_w 26 443 Da (bottom panel). Residual plots indicate the fit of the data to a given molecular weight. Very good fits are found in the top panel, indicating a correct assumption of the molecular weight; poor fits are found in the bottom panel and indicate an incorrect molecular-weight assumption.

Table 3: Double-Stranded DNA Oligonucleotides Used (AP1 Site Shown in Bold and Underlined)

oligo	sequence 5′−3′	stimulus	reference
CDK5	CGTCGG**TGACTCA**AAACAC	ECS, bitransgenic mice	*8*, *19*
MET	TCGACG**TGACTCA**GCGCGC	ECS, cocaine	*29*
GluR2	GACCCAG**TGACTAA**GGCAA	bitransgenic mice	*20*
SCR	GTATGCGATACGTCTTTCG		

Such an analysis of ΔFosB in a purified, isolated form is presented here for the first time. We show by mass spectrometry that ΔFosB produced in insect cells is not measurably post-translationally modified. In mammalian systems, ΔFosB undergoes phosphorylation at Ser27, which increases the stability and transcriptional activity of the protein (*5*, *50*). Our studies suggest that, because phosphorylation of ΔFosB does not occur by default in insect cells, eukaryotic cells that are routinely used to express recombinant phosphoproteins, post-translational modification of ΔFosB is a tightly regulated step and requires the presence of specific kinases.

Moreover, we show here that ΔFosB is capable of forming dimers in solution at submicromolar concentrations based on AUC experiments. In vitro studies exploring the ability of ΔFosB to heterodimerize with various Jun family proteins have previously indicated that ΔFosB can form heterodimers with JunB, c-Jun, and JunD (*51*−*54*). However, the interactions between Fos and Jun family proteins are heavily dependent upon the amounts of the different proteins produced and the potential partners available (*51*, *55*, *56*). The situation in vivo is more nebulous. The general thought is that chronic AP-1 complexes induced in the brain contain ΔFosB plus JunD predominantly, with a small amount of JunB but not c-Jun (*23*, *30*−*33*, *46*). However, the experiments supporting this notion have been technically limited. Interactions between ΔFosB and Jun family proteins have been studied with gel-shift assays of brain lysates probed with antibodies directed against various Fos and Jun family proteins. The results have not been straightforward to interpret, because anti-JunD antibodies in many studies only partially shifted or disrupted the chronic AP-1 complex or created novel species (*23*, *30*−*33*, *42*, *46*). This is very different compared to results with anti-ΔFosB antibodies or

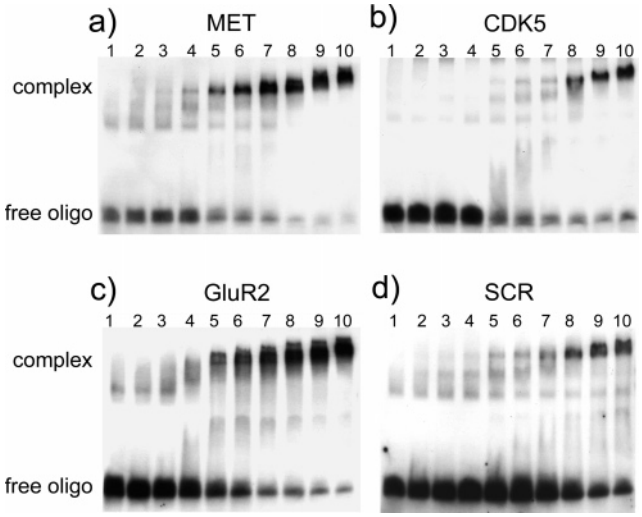

FIGURE 5: DNA-binding properties of N(His)$_6$ΔFosB. N(His)$_6$ΔFosB was incubated with four different double-stranded DNA oligos and analyzed with EMSAs. Shown are (a) MET AP-1, (b) CDK5 AP-1, (c) GluR2 AP-1, and (d) SCR. Fixed concentrations of DIG-labeled double-stranded oligo (50 nM) were incubated with increasing amounts of N(His)$_6$ΔFosB assuming a dimer (0, 26.3, 52.5, 78.8, 105, 131.3, 157.5, 210, 262.5, and 315 nM) and run on a native 6% acrylamide gel, and the chemiluminescent signal was detected as described in the Materials and Methods. Each sample contains 1 pmol of DIG-labeled oligo but varying amounts of protein (calculated as a dimer), namely, lane 1, no protein; lane 2, 0.5 pmol; lane 3, 1.1 pmol; lane 4, 1.6 pmol; lane 5, 2.1 pmol; lane 6, 2.6 pmol; lane 7, 3.2 pmol; lane 8, 4.2 pmol; lane 9, 5.3 pmol; and lane 10, 6.3 pmol. Bands indicating free oligo and complexed oligo are indicated.

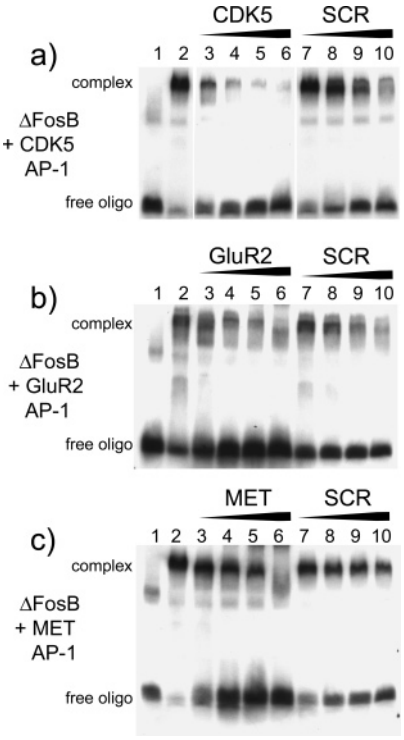

FIGURE 6: Specificity of DNA binding to N(His)$_6$ΔFosB. Three different protein/DNA complexes were formed by incubating 210 nM N(His)$_6$ΔFosB (dimer concentration) with 50 nM DIG-labeled oligo as described in the Materials and Methods. (a) CDK5 AP-1, (b) GluR2 AP-1, and (c) MET AP-1. Free specific oligo is shown in lane 1, and the protein/DNA complex is shown in lane 2. Competition was carried out by incubating the protein/DNA complexes with 10-, 50-, 200-, and 500-fold excess of unlabeled specific oligo (lanes 3−6) or an aspecific scrambled oligo SCR (lanes 7−10) to yield end-competitor concentrations of 500 nM (lanes 3 and 7), 2.5 μM (lanes 4 and 8), 10 μM (lanes 5 and 9), or 25 μM (lane 6 and 10), respectively. Samples were subsequently run on a native 6% acrylamide gel, and the chemiluminescent signal was detected as described in the Materials and Methods. Each sample contains 1 pmol of DIG-labeled oligo (lanes 1−10), 4.2 pmol of N(His)$_6$ΔFosB dimer (lanes 2−10), and different amounts of unlabeled specific or unspecific (SCR) competing oligo. Lane 3, 10 pmol of specific oligo; lane 4, 50 pmol of specific oligo; lane 5, 200 pmol of specific oligo; lane 6, 500 pmol of specific oligo; lane 7, 10 pmol of SCR oligo; lane 8, 50 pmol of SCR oligo; lane 9, 200 pmol of SCR oligo; and lane 10, 500 pmol of SCR oligo. Bands indicating free oligo and complexed oligo are indicated. Samples in part a originate from one blot but have been rearranged graphically to match the sample order of parts b and c, facilitating interpretation.

studies of fosB knockout mice, which completely abolish the chronic AP-1 binding activity (*23*, *30*, *31*, *57*). One possible explanation has been the lack of suitable anti-Jun antibodies. Other potential complications could be that chronic AP-1 complexes contain different components depending upon the radiolabeled oligonucleotides used to visualize the complex or the stimuli used to induce the chronic complex. Potentially more perplexing than the lack of a clear biochemically detectable interaction partner for ΔFosB is the finding that cells accumulating ΔFosB protein in response to chronic stimulation do not demonstrate significant levels of c-Jun or JunB mRNA or their encoded proteins (*58*, *59*), while JunD is constitutively expressed at relatively low levels and is not induced by acute or chronic stimulation (*23*, *32*, *33*, *60*). Our results suggest a hitherto unexplored possibility, namely, that ΔFosB forms homodimers in vivo upon attaining a threshold level of accumulation.

While this is the first study characterizing ΔFosB biochemically, there are some precedents for ΔFosB homodimerization being a legitimate possibility. Hallmark studies investigating the partner preference of peptides containing the c-Fos and c-Jun leucine zipper showed that, while c-Fos and c-Jun leucine zippers preferentially heterodimerize, homodimers of the c-Fos leucine zipper form at concentrations greater than 40 μM (*61*). The preferential formation of Fos/Jun heterodimers and Jun homodimers over Fos homodimers in vitro has been extended to other family members as well (*62*). However, the situation may be very different in vivo, where each cell type expresses a complex spectrum of bZIP proteins (including Fos, Jun, Maf, ATF, and CREB families) and, in addition to their partnering selectivity, their nuclear concentration and the presence of stabilizing co-activators ultimately dictate which components integrate into multiprotein transcription regulatory complexes (*55*, *56*). Hence, it is conceivable that the accumulation of ΔFosB to pathological levels in the subset of stimulated neurons could enable homodimer formation, a phenomenon that may not be observed under normal conditions.

The gel-shift and binding assays using fluorescence anisotropy show that ΔFosB can bind DNA in the absence of any Jun partner with roughly 100 nM affinity. Binding is specific based on competition with 10-fold unlabeled specific oligonucleotides but not a scrambled oligonucleotide. Earlier in vitro translation studies of various Fos and Jun partners, followed by gel-shift assays, have shown that ΔFosB (like FosB), in combination with JunB, c-Jun, or JunD, readily binds radiolabeled oligonucleotides containing an AP-1 site

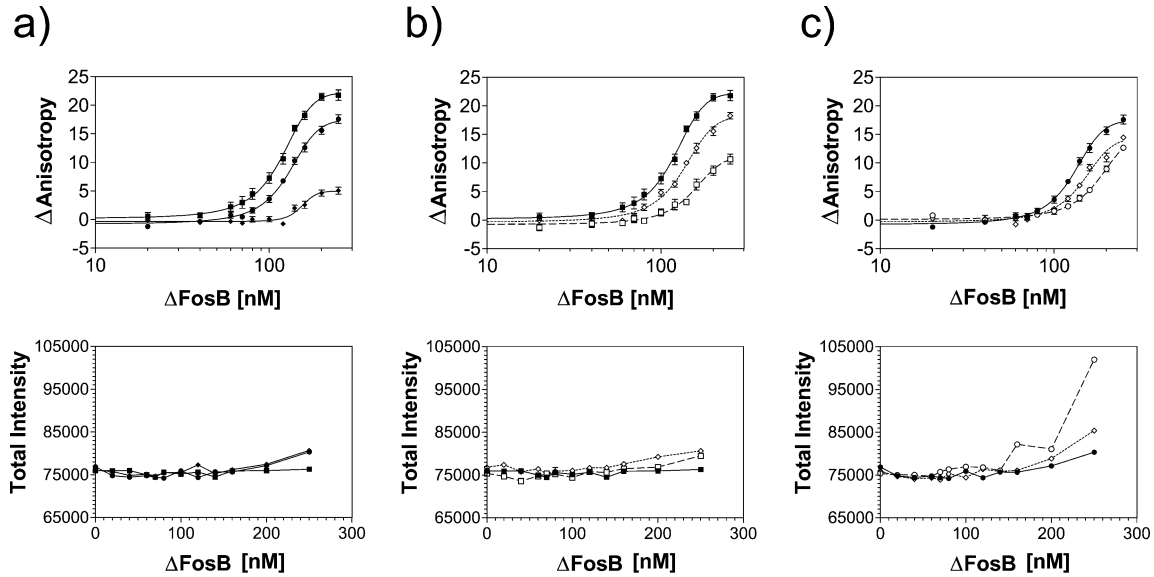

FIGURE 7: DNA-binding properties of N(His)$_6$ΔFosB assessed through fluorescence anisotropy. (a) TAMRA-labeled DNA oligos (50 nM) were incubated with increasing amounts of N(His)$_6$ΔFosB (0, 20, 40, 60, 70, 80, 100, 120, 140, 160, 200, and 250 nM dimer concentrations), and the change in the fluorescence anisotropic signal was monitored as a function of the protein concentration, as shown for TMR-CDK5 (■), TMR-GluR2 (●), and TMR-SCR (◆). (b) Increasing amounts of N(His)$_6$ΔFosB in the presence of 50 nM TMR-CDK5 (■, —), 50 nM TMR-CDK5 plus a 10-fold molar excess (i.e., 500 nM) of unlabeled CDK5 (□, - - -), and 50 nM TMR-CDK5 plus a 10-fold molar excess (i.e., 500 nM) of unlabeled SCR (◇, ···). (c) Increasing amounts of N(His)$_6$ΔFosB in the presence of 50 nM TMR-GluR2 (●, —), 50 nM TMR-GluR2 plus a 10-fold molar excess (i.e., 500 nM) of unlabeled GluR2 (○, - - -), and 50 nM TMR-GluR2 plus a 10-fold molar excess (i.e., 500 nM) of unlabeled SCR (◇, ···). For each experiment, the total fluorescence intensity is shown as well; error bars, while displayed, are not visible because the standard error of the mean is less than 1.5% for all data points. The total fluorescence intensity does not change more than 7% over the course of each experiment (with the exception of two data points in c), indicating that changes in fluorescence anisotropy are primarily due to slower tumbling of the fluorescent oligo (i.e., protein binding) and not environmental changes promoting altered emission.

(*51*, *52*). In these studies, DNA binding by ΔFosB or FosB alone was not observed, although under these conditions, Jun family proteins do not bind DNA alone either. It is well-established that Jun family proteins bind DNA as homodimers at low nanomolar concentrations. Heterodimerization with Fos family proteins increases the binding affinity for AP-1 sites approximately 10-fold, although heterodimers appear to have less transcriptional activity (*51*, *63*). Our results indicate that ΔFosB homodimers have a preference for certain AP-1 sites containing oligonucleotides (Figures 6 and 7), which demonstrates that the 7 nucleotide AP-1 consensus sequence alone is not sufficient to explain binding specificity, an observation previously made for AP-1 complexes induced by various stimuli in vivo (*18*, *29*, *59*) and generated by Fos/Jun and Jun complexes in vitro (*64*). Interestingly, the binding of ΔFosB to DNA appears cooperative (Figure 7), which suggests that DNA-binding and dimerization potentials may be unleashed at similar concentrations of ΔFosB and that the actual levels to which ΔFosB accumulates in response to chronic stimuli in the nucleus are important.

The ability of ΔFosB homodimers to bind DNA in vitro and therefore potentially in vivo as well has consequences for understanding how ΔFosB regulates gene expression. Studies to date have demonstrated that ΔFosB can serve as a transcriptional repressor and activator both in vitro and in vivo (*8*, *9*, *18*, *51*−*53*). This work has suggested that the transcriptional effects of ΔFosB depend upon several factors, including the particular gene involved, the Jun partners present, the relative amounts of ΔFosB and its potential binding partners, and the cell type in question. Inducible overexpression of ΔFosB in bitransgenic adult mice have shown that, at lower expression levels, ΔFosB functions predominantly as a transcriptional repressor, while at higher levels, it functions predominantly as a transcriptional activator when its primary behavioral effects become manifest (*9*). Our results raise the possibility that, as ΔFosB levels accumulate in the brain in response to chronic stimulation, they may pass a threshold at which homodimerization occurs in the cell, forming a unique transcription factor that mediates long-term neural and behavioral plasticity. If so, this discovery could have important implications in exploiting ΔFosB in the development of new treatments for psychiatric and neurological diseases.

ACKNOWLEDGMENT

We thank Steve Afendis and Bikash Pramanik at the UT Southwestern Medical Center for their help with mass spectrometric analyses and most gratefully acknowledge Prof. Johann Deisenhofer for the opportunity to start this work in his laboratory. Helpful discussions with Dr. Tom Kerppola, Dr. David Akey, and Martha Larsen are gratefully acknowledged as well.

REFERENCES

1. Morgan, J. I., and Curran, T. (1995) Immediate-early genes: Ten years on, *Trends Neurosci. 18*, 66−67.
2. Rylski, M., and Kaczmarek, L. (2004) Ap-1 targets in the brain, *Front. Biosci. 9*, 8−23.
3. Nestler, E. J., Barrot, M., and Self, D. W. (2001) ΔFosB: A sustained molecular switch for addiction, *Proc. Natl. Acad. Sci. U.S.A. 98*, 11042−11046.
4. McClung, C. A., Ulery, P. G., Perrotti, L. I., Zachariou, V., Berton, O., and Nestler, E. J. (2004) ΔFosB: A molecular switch for long-term adaptation in the brain, *Brain Res. Mol. Brain Res. 132*, 146−154.

5. Ulery, P. G., Rudenko, G., and Nestler, E. J. (2006) Regulation of ΔFosB stability by phosphorylation, *J. Neurosci. 26*, 5131−5142.
6. Alibhai, I. N., Green, T. A., and Nestler, E. J. (2007) Regulation of fosB and ΔfosB mRNA expression: In vivo and in vitro studies, *Brain Res.*, in press.
7. Carle, T. L., Alibhai, I. N., Wilkinson, M. B., Kumar, A., and Nestler, E. J. (2007) Proteasome dependent and independent mechanisms for FosB destabilization: Identification of FosB degradation domains and implications for ΔFosB stability, *Eur. J. Neurosci.*, manuscript in revision.
8. Kumar, A., Choi, K. H., Renthal, W., Tsankova, N. M., Theobald, D. E., Truong, H. T., Russo, S. J., Laplant, Q., Sasaki, T. S., Whistler, K. N., Neve, R. L., Self, D. W., and Nestler, E. J. (2005) Chromatin remodeling is a key mechanism underlying cocaine-induced plasticity in striatum, *Neuron 48*, 303−314.
9. McClung, C. A., and Nestler, E. J. (2003) Regulation of gene expression and cocaine reward by CREB and ΔFosB, *Nat. Neurosci. 6*, 1208−1215.
10. Pace, C. N., Vajdos, F., Fee, L., Grimsley, G., and Gray, T. (1995) How to measure and predict the molar absorption coefficient of a protein, *Protein Sci. 4*, 2411−2423.
11. Laue, T. M., Shah, B. D., Ridgeway, T. M., and Pelletier, S. L. (1992) Computer-aided interpretation of sedimentation data for proteins, in *Analytical Ultracentrifugation in Biochemistry and Polymer Science* (Harding, S. E., Rowe, A. J., and Horton, J. C., Eds.) pp 90−125, The Royal Society of Chemistry, Cambridge, U.K.
12. Stafford, W. F., Walker, M. L., Trinick, J. A., and Coluccio, L. M. (2005) Mammalian class I myosin, Myo1b, is monomeric and cross-links actin filaments as determined by hydrodynamic studies and electron microscopy, *Biophys. J. 88*, 384−391.
13. Schuck, P. (2000) Size-distribution analysis of macromolecules by sedimentation velocity ultracentrifugation and lamm equation modeling, *Biophys. J. 78*, 1606−1619.
14. Schuck, P. (2005) In *Modern Analytical Ultracentrifugation: Techniques and Methods* (Scott, D. J., Harding, S. E., and Rowe, A. J., Eds.) The Royal Society of Chemistry, Cambridge, U.K.
15. Vistica, J., Dam, J., Balbo, A., Yikilmaz, E., Mariuzza, R. A., Rouault, T. A., and Schuck, P. (2004) Sedimentation equilibrium analysis of protein interactions with global implicit mass conservation constraints and systematic noise decomposition, *Anal. Biochem. 326*, 234−256.
16. Hu, C. C., and Ghabrial, S. A. (1995) The conserved, hydrophilic and arginine-rich N-terminal domain of cucumovirus coat proteins contributes to their anomalous electrophoretic mobilities in sodium dodecylsulfate−polyacrylamide gels, *J. Virol. Methods 55*, 367−379.
17. Graceffa, P., Jancsó, A., and Mabuchi, K. (1992) Modification of acidic residues normalizes sodium dodecyl sulfate−polyacrylamide gel electrophoresis of caldesmon and other proteins that migrate anomalously, *Arch. Biochem. Biophys. 297*, 46−51.
18. Chen, J., Kelz, M. B., Hope, B. T., Nakabeppu, Y., and Nestler, E. J. (1997) Chronic Fos-related antigens: Stable variants of ΔFosB induced in brain by chronic treatments, *J. Neurosci. 17*, 4933−4941.
19. Chen, J., Zhang, Y., Kelz, M. B., Steffen, C., Ang, E. S., Zeng, L., and Nestler, E. J. (2000) Induction of cyclin-dependent kinase 5 in the hippocampus by chronic electroconvulsive seizures: Role of ΔFosB, *J. Neurosci. 20*, 8965−8971.
20. Kelz, M. B., Chen, J., Carlezon, W. A., Jr., Whisler, K., Gilden, L., Beckmann, A. M., Steffen, C., Zhang, Y. J., Marotti, L., Self, D. W., Tkatch, T., Baranauskas, G., Surmeier, D. J., Neve, R. L., Duman, R. S., Picciotto, M. R., and Nestler, E. J. (1999) Expression of the transcription factor ΔFosB in the brain controls sensitivity to cocaine, *Nature 401*, 272−276.
21. Hope, B. T., Nye, H. E., Kelz, M. B., Self, D. W., Iadarola, M. J., Nakabeppu, Y., Duman, R. S., and Nestler, E. J. (1994) Induction of a long-lasting AP-1 complex composed of altered Fos-like proteins in brain by chronic cocaine and other chronic treatments, *Neuron 13*, 1235−1244.
22. Couceyro, P., Pollock, K. M., Drews, K., and Douglass, J. (1994) Cocaine differentially regulates activator protein-1 mRNA levels and DNA-binding complexes in the rat striatum and cerebellum, *Mol. Pharmacol. 46*, 667−676.
23. Chen, J., Nye, H. E., Kelz, M. B., Hiroi, N., Nakabeppu, Y., Hope, B. T., and Nestler, E. J. (1995) Regulation of ΔFosB and FosB-like proteins by electroconvulsive seizure and cocaine treatments, *Mol. Pharmacol. 48*, 880−889.
24. Moratalla, R., Elibol, B., Vallejo, M., and Graybiel, A. M. (1996) Network-level changes in expression of inducible Fos−Jun proteins in the striatum during chronic cocaine treatment and withdrawal, *Neuron 17*, 147−156.
25. Nye, H. E., and Nestler, E. J. (1996) Induction of chronic Fos-related antigens in rat brain by chronic morphine administration, *Mol. Pharmacol. 49*, 636−645.
26. Muller, D. L., and Unterwald, E. M. (2005) D1 dopamine receptors modulate ΔFosB induction in rat striatum after intermittent morphine administration, *J. Pharmacol. Exp. Ther. 314*, 148−154.
27. McDaid, J., Dallimore, J. E., Mackie, A. R., and Napier, T. C. (2006) Changes in accumbal and pallidal pCREB and ΔFosB in morphine-sensitized rats: Correlations with receptor-evoked electrophysiological measures in the ventral pallidum, *Neuropsychopharmacology 31*, 1212−1226.
28. Radwanska, K., Valjent, E., Trzaskos, J., Caboche, J., and Kaczmarek, L. (2006) Regulation of cocaine-induced activator protein 1 transcription factors by the extracellular signal-regulated kinase pathway, *Neuroscience 137*, 253−264.
29. Hope, B. T., Kelz, M. B., Duman, R. S., and Nestler, E. J. (1994) Chronic electroconvulsive seizure (ECS) treatment results in expression of a long-lasting AP-1 complex in brain with altered composition and characteristics, *J. Neurosci. 14*, 4318−4328.
30. Mandelzys, A., Gruda, M. A., Bravo, R., and Morgan, J. I. (1997) Absence of a persistently elevated 37 kDa fos-related antigen and AP-1-like DNA-binding activity in the brains of kainic acid-treated fosB null mice, *J. Neurosci. 17*, 5407−5415.
31. Hiroi, N., Marek, G. J., Brown, J. R., Ye, H., Saudou, F., Vaidya, V. A., Duman, R. S., Greenberg, M. E., and Nestler, E. J. (1998) Essential role of the fosB gene in molecular, cellular, and behavioral actions of chronic electroconvulsive seizures, *J. Neurosci. 18*, 6952−6962.
32. Morris, T. A., Jafari, N., and DeLorenzo, R. J. (2000) Chronic ΔFosB expression and increased AP-1 transcription factor binding are associated with the long term plasticity changes in epilepsy, *Brain Res. Mol. Brain Res. 79*, 138−149.
33. Vallone, D., Pellecchia, M. T., Morelli, M., Verde, P., DiChiara, G., and Barone, P. (1997) Behavioural sensitization in 6-hydroxydopamine-lesioned rats is related to compositional changes of the AP-1 transcription factor: Evidence for induction of FosB- and JunD-related proteins, *Brain Res. Mol. Brain Res. 52*, 307−317.
34. Hiroi, N., and Graybiel, A. M. (1996) Atypical and typical neuroleptic treatments induce distinct programs of transcription factor expression in the striatum, *J. Comp. Neurol. 374*, 70−83.
35. Atkins, J. B., Chlan-Fourney, J., Nye, H. E., Hiroi, N., Carlezon, W. A., Jr., and Nestler, E. J. (1999) Region-specific induction of ΔFosB by repeated administration of typical versus atypical antipsychotic drugs, *Synapse 33*, 118−128.
36. Kontkanen, O., Lakso, M., Wong, G., and Castren, E. (2002) Chronic antipsychotic drug treatment induces long-lasting expression of fos and jun family genes and activator protein 1 complex in the rat prefrontal cortex, *Neuropsychopharmacology 27*, 152−162.
37. Bing, G., Wang, W., Qi, Q., Feng, Z., Hudson, P., Jin, L., Zhang, W., Bing, R., and Hong, J. S. (1997) Long-term expression of Fos-related antigen and transient expression of ΔFosB associated with seizures in the rat hippocampus and striatum, *J. Neurochem. 68*, 272−279.
38. Perez-Otano, I., Mandelzys, A., and Morgan, J. I. (1998) MPTP-Parkinsonism is accompanied by persistent expression of a ΔFosB-like protein in dopaminergic pathways, *Brain Res. Mol. Brain Res. 53*, 41−52.
39. Andersson, M., Westin, J. E., and Cenci, M. A. (2003) Time course of striatal ΔFosB-like immunoreactivity and prodynorphin mRNA levels after discontinuation of chronic dopaminomimetic treatment, *Eur. J. Neurosci. 17*, 661−666.
40. Perrotti, L. I., Hadeishi, Y., Ulery, P. G., Barrot, M., Monteggia, L., Duman, R. S., and Nestler, E. J. (2004) Induction of ΔFosB in reward-related brain structures after chronic stress, *J. Neurosci. 24*, 10594−10602.
41. Colby, C. R., Whisler, K., Steffen, C., Nestler, E. J., and Self, D. W. (2003) Striatal cell type-specific overexpression of ΔFosB enhances incentive for cocaine, *J. Neurosci. 23*, 2488−2493.
42. Peakman, M. C., Colby, C., Perrotti, L. I., Tekumalla, P., Carle, T., Ulery, P., Chao, J., Duman, C., Steffen, C., Monteggia, L.,

Allen, M. R., Stock, J. L., Duman, R. S., McNeish, J. D., Barrot, M., Self, D. W., Nestler, E. J., and Schaeffer, E. (2003) Inducible, brain region-specific expression of a dominant negative mutant of c-Jun in transgenic mice decreases sensitivity to cocaine, *Brain Res. 970*, 73−86.

43. Zachariou, V., Bolanos, C. A., Selley, D. E., Theobald, D., Cassidy, M. P., Kelz, M. B., Shaw-Lutchman, T., Berton, O., Sim-Selley, L. J., Dileone, R. J., Kumar, A., and Nestler, E. J. (2006) An essential role for ΔFosB in the nucleus accumbens in morphine action, *Nat. Neurosci. 9*, 205−211.
44. Andersson, M., Hilbertson, A., and Cenci, M. A. (1999) Striatal fosB expression is causally linked with L-DOPA-induced abnormal involuntary movements and the associated upregulation of striatal prodynorphin mRNA in a rat model of Parkinson's disease, *Neurobiol. Dis. 6*, 461−474.
45. Cenci, M. A., Tranberg, A., Andersson, M., and Hilbertson, A. (1999) Changes in the regional and compartmental distribution of FosB- and JunB-like immunoreactivity induced in the dopamine-denervated rat striatum by acute or chronic L-DOPA treatment, *Neuroscience 94*, 515−527.
46. Andersson, M., Konradi, C., and Cenci, M. A. (2001) cAMP response element-binding protein is required for dopamine-dependent gene expression in the intact but not the dopamine-denervated striatum, *J. Neurosci. 21*, 9930−9943.
47. Cenci, M. A. (2002) Transcription factors involved in the pathogenesis of L-DOPA-induced dyskinesia in a rat model of Parkinson's disease, *Amino Acids 23*, 105−109.
48. Carlsson, T., Winkler, C., Burger, C., Muzyczka, N., Mandel, R. J., Cenci, A., Bjorklund, A., and Kirik, D. (2005) Reversal of dyskinesias in an animal model of Parkinson's disease by continuous L-DOPA delivery using rAAV vectors, *Brain 128*, 559−569.
49. Berton, O., Tsankova, N. M., Carle, T. L., Ulery, P. G., Bhonsle, A., Barrot, M., Neve, R. L., and Nestler, E. J. (2007) Induction of ΔFosB in the periaqueductal gray by stress promotes active coping responses, *Neuron*, manuscript in revision.
50. Ulery, P. G., and Nestler, E. J. (2007) Regulation of ΔFosB transcriptional activity by Ser27 phosphorylation, *Eur. J. Neurosci. 25*, 224−230.
51. Nakabeppu, Y., and Nathans, D. (1991) A naturally occurring truncated form of FosB that inhibits Fos/Jun transcriptional activity, *Cell 64*, 751−759.
52. Yen, J., Wisdom, R. M., Tratner, I., and Verma, I. M. (1991) An alternative spliced form of FosB is a negative regulator of transcriptional activation and transformation by Fos proteins, *Proc. Natl. Acad. Sci. U.S.A. 88*, 5077−5081.
53. Dobrazanski, P., Noguchi, T., Kovary, K., Rizzo, C. A., Lazo, P. S., and Bravo, R. (1991) Both products of the fosB gene, FosB and its short form, FosB/SF, are transcriptional activators in fibroblasts, *Mol. Cell. Biol. 11*, 5470−5478.
54. Wisdom, R., and Verma, I. M. (1993) Proto-oncogene FosB: The amino terminus encodes a regulatory function required for transformation, *Mol. Cell. Biol. 13*, 2635−2643.
55. Chinenov, Y., and Kerppola, T. K. (2001) Close encounters of many kinds: Fos−Jun interactions that mediate transcription regulatory specificity, *Oncogene 20*, 2438−2452.
56. Hess, J., Angel, P., and Schorpp-Kistner, M. (2004) AP-1 subunits: Quarrel and harmony among siblings, *J. Cell Sci. 117*, 5965−5973.
57. Hiroi, N., Brown, J. R., Haile, C. N., Ye, H., Greenberg, M. E., and Nestler, E. J. (1997) FosB mutant mice: Loss of chronic cocaine induction of Fos-related proteins and heightened sensitivity to cocaine's psychomotor and rewarding effects, *Proc. Natl. Acad. Sci. U.S.A. 94*, 10397−10402.
58. Winston, S. M., Hayward, M. D., Nestler, E. J., and Duman, R. S. (1990) Chronic electroconvulsive seizures down-regulate expression of the immediate-early genes c-fos and c-jun in rat cerebral cortex, *J. Neurochem. 54*, 1920−1925.
59. Hope, B., Kosofsky, B., Hyman, S. E., and Nestler, E. J. (1992) Regulation of immediate early gene expression and AP-1 binding in the rat nucleus accumbens by chronic cocaine, *Proc. Natl. Acad. Sci. U.S.A. 89*, 5764−5768.
60. Valastro, B., Andersson, M., Lindgren, H. S., and Cenci, M. A. (2007) Expression pattern of JunD after acute or chronic l-DOPA treatment: Comparison with ΔFosB, *Neuroscience 144*, 198−207.
61. O'Shea, E. K., Rutkowski, R., Stafford, W. F., III, and Kim, P. S. (1989) Preferential heterodimer formation by isolated leucine zippers from fos and jun, *Science 245*, 646−648.
62. Vinson, C., Myakishev, M., Acharya, A., Mir, A. A., Moll, J. R., and Bonovich, M. (2002) Classification of human B-ZIP proteins based on dimerization properties, *Mol. Cell. Biol. 22*, 6321−6335.
63. Nakabeppu, Y., Ryder, K., and Nathans, D. (1988) DNA binding activities of three murine Jun proteins: Stimulation by Fos, *Cell 55*, 907−915.
64. Ryseck, R. P., and Bravo, R. (1991) c-JUN, JUN B, and JUN D differ in their binding affinities to AP-1 and CRE consensus sequences: Effect of FOS proteins, *Oncogene 6*, 533−542.

BI700494V